Oscillation-induced Softening in Copper and Molybdenum from Nano- to Micro-length Scales

K.W. Siu and A.H.W. Ngan[§]

Department of Mechanical Engineering, The University of Hong Kong,

Pokfulam Road, Hong Kong, P.R. China

([§]Corresponding Author, email: hwngan@hku.hk)

Abstract

That the application of a simultaneous oscillatory stress can lead to significant reductions in the quasi-static stress required to sustain deformation has found a wide range of industrial applications. Recently, we discovered that, in addition to the widely believed effects of stress superposition, the oscillation-induced softening in aluminium is an intrinsic effect associated with enhanced dislocation annihilation and subgrain formation arising from the simultaneous oscillatory stress. However, such intrinsic effects have not been proven as a general phenomenon for other metals. In this study, macroscopic and nano-indentation were performed on copper and molybdenum. The results show that the simultaneous application of oscillatory stresses can lower the hardness of these samples. EBSD and TEM observations show that subgrain formation and reduction in dislocation density generally occurred when stress oscillations were

applied. These suggest that the intrinsic oscillation-induced effects of softening and dislocation annihilation are a rather general phenomenon occurring in metals with different stacking fault energies and crystal structures.

Keywords: acoustoplasticity; nanoindentation; hardness; subgrains; dislocation annihilation

1. Introduction

The phenomenon that vibration can lower the quasi-static loading stress required to sustain deformation has been observed and studied first as “acoustoplasticity” in the macro-scale. Acoustoplasticity is also known as the Blaha effect, or ultrasonic softening [1, 2], and it can be defined as a reduction in the quasi-static stress required to deform a material as ultrasonic vibration is simultaneously applied. Acoustoplasticity is utilized in many different industrial processes to deform, cut or join metals [3-10], and is a phenomenon widely investigated over the last sixty years using tensile, compression or other test modes [1, 2, 11-28] .

Besides the macroscopic softening due to the application of ultrasonic vibration, the lowering of loading due to the presence of an oscillatory stress in the nano-scale has also been observed in nanoindentation experiments. Commercially available nanoindentation instruments are usually equipped with the continuous stiffness measurement (CSM) mode of operation [29-33], in which an oscillatory load signal is superimposed on a background, slowly varying quasi-static load schedule of the indenter tip. Durst et al. [34] found that the hardness of nickel single crystals obtained using CSM is significantly lower than that obtained with quasi-static mode,

while the hardness obtained using the quasi-static mode exhibited the usual indentation size effect, the difference in hardness obtained using the quasi-static and CSM modes increased with smaller indent depths. Cordill et al. [35-37] found that for the same displacement, the measured load on nickel was lower in the CSM mode than in the quasi-static mode, especially for the first 200 nm of the indenter's displacement. Pharr et al. [38] found that the extent of load reduction in copper under CSM increased with the oscillation amplitude, and that the measured modulus and hardness data decreased with increasing oscillation amplitude. Similar to other studies these effects were found to diminish as the indent depth increased.

The conventional understanding of macroscopic acoustoplasticity can be divided into two main theories. One is that such softening is due to an increase of the dislocation mobility caused by the vibration excitation, which increases their ability to overcome obstacles [1, 2]. The other, adopted mainly by continuum-plasticity researchers, is a superposition theory in which the same yield surface of the material is assumed but since the oscillatory stress reinforces the quasi-static stress in one half of the stress cycle, a lower quasi-static stress would be required to maintain yielding at the same criteria when compared to the case without the oscillatory stress [39, 40]. Based on this theory, a model has also been developed [39] by assuming the dislocation

density and the relation between strain rate and stress being unchanged, and with the presence of an oscillatory stress, a smaller static stress is required to deform the material at the same strain rate, compared to the case without simultaneous application of oscillation.

For the nano-scale softening mentioned above, Cordill et al. [37] named the phenomenon as “nano-jackhammer effect”, and proposed that the overall response in the CSM mode nanoindentation is a result of a competition between two opposite effects, (i) a hardening effect due to a higher effective strain rate caused by the superimposed oscillation, and (ii) a softening effect due to enhancement of dislocation nucleation caused by the imposed oscillatory stress. The resultant softening is due to the domination of the softening effect in (ii). On the other hand, Pharr et al. [38] attributed these effects to instrumental and measurement errors and suggested different correction methods. The above are two different approaches to interpret the nano-scale vibration-induced softening effect: Cordill et al.’s proposal [37] is an intrinsic softening effect in which the material’s response is intrinsically altered through enhancement of the nucleation of dislocations or promotion of their speed by the vibrations, while Pharr et al.’s interpretation [38] focuses on instrumental or experimental errors, and these,

together with the above-mentioned superposition theory, may be referred to as extrinsic effects.

Despite the considerable experimental and modelling efforts of previous researchers, there is still no clear and comprehensive understanding on the mechanism of vibration-induced softening in both macro- and nano-scale. In particular, it is still uncertain whether the effect of an oscillatory stress on metal plasticity is extrinsic or intrinsic. In a recent study [41], we found that very extensive subgrain formation occurred in bulk aluminium samples if ultrasonic vibration was simultaneously applied to quasi-static macro-indentation, while no subgrain formation was found in quasi-static indentation alone. More recently using aluminium samples, a similar phenomenon was also observed in nanoindentation [42]: subgrain formation was enhanced in the CSM mode, and even with the load corrections introduced by Pharr et al. [38] applied and with the hardness calculated directly from the imaged indent sizes, significant softening still existed in the CSM mode, indicating that the softening effect is intrinsic. Dislocation dynamics simulations also revealed that dipole annihilation is particularly enhanced in the presence of a superimposed oscillatory stress, because the dislocations are made to travel longer distances in a jerky manner [43]. Similarly, in CSM nanoindentation, during the unloading half cycle, stress is relieved as a result of

elastic recovery from an elastoplastic state, and hence reversals in dislocation motion may occur. These motion reversals should allow dislocations to explore more and hence increase their chance of dipole annihilation, leading to a reduction in the flow stress [42].

Although the previous observations indicate that oscillatory stresses can produce an intrinsic softening effect in aluminium, it is not clear whether such an effect is a more general phenomenon. Al is a high stacking-fault-energy (SFE) FCC metal in which cross-slip and other obstacle by-passing mechanisms are particularly easy. In this work, two different metals, copper and molybdenum, were subjected to the same investigations to see if similar intrinsic softening also occurs with oscillations. Cu is a low SFE FCC metal which would provide a check to see if the observations made on Al above are unique to low SFE metals. Mo has BCC structure, and so would provide clues on whether the observed softening effects are crystal structure sensitive.

2. Experimental details

2.1 Sample preparation

The bulk materials used in this investigation were polycrystalline copper and molybdenum of ~99.9 wt. % purity. Square pieces with approximate dimensions

10×10×3 mm were cut from the bulk materials. The copper samples were annealed at 900^{o}C for 24 hours, and the resultant grain size was about 200 μm on average. The molybdenum samples were annealed at 1200^{o}C for 48 hours, and the resultant grain size was about 25 μm on average. The samples were then mechanically polished with silicon carbide paper and diamond paste down to 1 μm, the copper samples were then electropolished using an electrolyte of 30% phosphoric acid in distilled water using a voltage of 1.6 V d.c. for about 3 minutes, while the molybdenum samples were electropolished using an electrolyte of 10% concentrated sulphuric acid in acetic acid using a voltage of 17 V d.c. for about 3 minutes.

2.2 Macroscopic indentation

In macroscopic indentation, the same experimental setup as in our previous work on Al [41] was used. In these experiments, the specimen was glued onto the upper surface near the tip of a sonotrode, which is the vibrating part of the set up. Ultrasonic vibration was provided by an ultrasonic generator which can generate signals with frequencies of about 30 kHz. The transducer connecting to the generator converted the signal to uni-directional mechanical vibrations of the sonotrode. The sonotrode, onto which the sample was stuck, set the sample into horizontal vibrations with amplitudes from 2 to 10 μm. The sonotrode/specimen assembly was then placed underneath a

Buehler Micromat 2100 hardness tester equipped with a Vickers diamond indenter tip. Different vibration amplitudes (0 μm, 2 μm, 6 μm, 10 μm) and indenter loads (0.05 kg, 0.1 kg, 0.2 kg, 0.3 kg) were used and five indents were made for each combination of generator current and indenter load. The corresponding residual indent sizes were recorded for calculation and comparison.

2.3 Nanoindentation

Nanoindentation tests were performed on copper and molybdenum samples using an Agilent NanoIndenter G200 system with a Berkovich indenter. The nanoindentation was carried out in both the quasi-static mode and CSM mode using a constant indentation strain rate of $\dot{P}/P = 0.05\ s^{-1}$, and different CSM amplitudes of 2 nm, 4 nm, 8 nm and 12 nm, and final indent depths of 200 nm, 700 nm, 1200 nm, 1700nm and 2000 nm, were used. Nine indents were made for each combination of amplitude and indent depth. The CSM frequency was 45 Hz. For copper the results were all gathered from a single grain with normal orientation of [101] as identified by electron backscattered diffraction (EBSD) in a Leo 1530 FEG scanning electron microscope (SEM). For Molybdenum since the grain size is small it was impossible for all the indents to be made in one single grain to obtain an identical grain orientation condition, and in fact the indents may cover more than one grain. The results for

molybdenum here therefore represent the general observation in a polycrystalline context.

2.4 Hardness calculation

For the macroscopic indentation hardness, the conventional way of using the residual indent's diagonal length to calculate the Vickers hardness as $H_v = 1.86P/d^2$ [44] was adopted. For nanoindentation hardness, since the tip may lose contact with the sample at shallow depths [38], the hardness values directly reported from the machine's software are not accurate. Although correction methods have been proposed [38], it was shown that the corrected values still deviate from the corrected SEM hardness [42]. Therefore in this study only corrected SEM hardness are reported. Residual indents were imaged using SEM. The projected indent areas were measured by tracing the indent periphery and counting the pixels inside the periphery with the help of image processing software. Then the area is used in calculating the hardness as the corrected peak indentation load at maximum depth divided by the indent area, as done in [42].

2.5 Microscopic investigation

Both macro- and nano-indents were extracted for microscopic investigation. For macro-indents, cross-sectional foils of the indents were cut out from the specimens

along the indent diagonals by focused ion beam (FIB) milling in an FEI Quanta 200 3D FIB system. To do this, two ditches were milled to leave a foil of about 3 μm thick in between. The foil was then freed from the sample by FIB cutting along its perimeter, and this was then attached onto a copper grid by tungsten soldering inside the FIB. The foil was then further fine-polished by FIB using a reduced ion current to enhance the surface quality. The foil was then investigated by EBSD. Then the cross-sectional foils made this way were further thinned down to about 100nm by FIB for inspection in a Tecnai G2 20 S-Twin TEM. Nano-indents were also cut out in a similar manner and investigated using TEM.

3. Results

3.1 Macroscopic indentation

Fig. 1 shows how the indent diagonal length and the hardness vary with the vibration amplitude of the sample. Here, the vibration provided by the sonotrode is mostly in the horizontal in-plane direction, and zero vibration amplitude means no vibration was applied to the sample. For all indentation loads from 0.05 kg to 0.3 kg in the normal, vertical direction, an increasing trend of softening can be observed with increasing vibration amplitude for both copper and molybdenum. Compared to indentations without vibration, a significant increase in diagonal length can be obtained

even with a small vibration amplitude of 2 μm, and in all cases, the increase in diagonal length is much larger than the vibration amplitude applied to the sample. For example, in the 0.05 kg indentation load for copper sample, the diagonal length increases from 50 μm to 150 μm with only a small in-plane vibration amplitude of about 2 μm, as shown in Fig. 1(a). A similar phenomenon also occurs in molybdenum – a 2 μm amplitude leads to an increase of diagonal length from 20 μm to 85 μm, as shown in Fig. 1(b). Furthermore, as noted previously for Al [41], the indents with vibrations were found to remain isotropic in shape in the plan view for both Cu and Mo, indicating that the in-plane vibrations provided by the sonotrode produced softening in the material allowing the loaded indenter to sink further into the sample in the vertical direction, rather than scratching in the in-plane direction, which would have resulted in elongated indent shapes.

Fig. 2(a) and (b) show the EBSD orientation map of cross-sectional foils cut from indents of copper made by 0.05 kg load without and with 2 μm vibration respectively, while Fig. 2(c) and (d) show their counterparts for molybdenum sample. Fig. 2(a) and (c) does not reveal any large variation in the crystal orientation within the sample, confirming similar orientation within the foils. On the contrary Fig. 2(b) and (d) show that many tiny regions with clear boundaries and sharp contrast can be seen,

showing the existence of subgrains with rather large misorientations. Fig. 2(b) shows that the size of these subgrains is about 0.3 to 0.5 μm for copper, while Fig. 2(d) shows that subgrains in molybdenum are about 1 to 2 μm large. The inverse pole figure legend shown in Fig 2(a) is applicable to all the EBSD orientation maps in this paper.

Fig. 3(a) and (b) show the TEM montages of parts of the cross-sectional foils cut from indents of copper made by 0.05 kg load without and with 2 μm vibration respectively, while Fig. 3(c) and (d) show their counterparts for molybdenum. In Fig. 3(a), which shows a part of the foil of copper without vibration, dense dislocations forming entanglements and networks are visible, but no subgrain structure is revealed. The inset shows a magnified part of the sample and reveals a dislocation density on the order of 10^{15} m^{-2}. On the contrary, a very remarkable difference in the tendency of subgrain formation can be seen from the vibrated indent of copper, as shown in Fig. 3(b). Here, subgrains can be clearly seen and they also exhibit very different contrast amongst themselves; from the inset, the dislocation density within a subgrain is at a lower order of magnitude of about 10^{14} m^{-2}. As in the EBSD orientation mapping, Fig. 3(c) does not show any subgrain in the non-vibrated molybdenum sample but clear subgrain can be observed in the vibrated one shown in Fig. 3(d) – in this case the

dislocation density in the vibrated sample is about 10^{13} m^{-2}, lower than the 10^{14} m^{-2} in the non-vibrated case.

3.2 Nanoindentation

Fig. 4(a) and (b) show the representative load-displacement curves of nanoindentation tests under the quasi-static mode and CSM mode with different amplitudes for copper and molybdenum respectively. In each condition in Fig. 4, a typical curve from the nine repeated measurements is shown. The main panels in Fig. 4(a) and (b) show data up to 2000 nm of indentation depth, and from these broader views the difference in loading, especially at larger depths, is not obvious. However, the magnified view in the inset of Fig. 4(a) reveals that a significant reduction of loading occurs under the CSM mode for copper, and the extent of softening increases with increasing CSM amplitude. For molybdenum Fig. 4(b) shows that although the lowering of loading is less obvious than that in copper, softening can still be observed for the larger amplitude of 12 nm. As mentioned before, the softening in CSM nanoindentation is also observed in previous studies by other researchers on other metals [35-37, 42].

In Fig. 5(a) and (b) the hardness data with different CSM amplitudes for copper and molybdenum are compared with those obtained using quasi-static mode of indentation. Here, to avoid the various instrumental errors discussed by Pharr et al. [38] from affecting the results, the hardness data were calculated from the imaged projected areas A_{SEM} of the indents as seen in the scanning electron microscope (SEM) [42], namely,

$$H = P_{act} / A_{SEM} . \quad (1)$$

With the CSM mode, the true mean load applied P_{act} also takes into account the effect of the oscillations according to Pharr et al. [38], namely,

$$P_{act} = P_{app} + \sqrt{2}\Delta P_{rms}, \quad (2)$$

where ΔP_{rms} is the root-mean-squared amplitude of the CSM oscillations, and P_{app} is the quasi-static load applied. At certain shallow indent depths, the indenter tip may lose contact with the sample due to the relatively large amplitude of vibration [38], and whenever this occurs the load recorded by the machine is doubtful; such data are circled in Fig. 5. However, even if these doubtful data in the "woodpecker" regime [38] in Fig. 5(a) and (b) are ignored, the hardness with the CSM mode switched on still exhibits significantly lower values for small indent depths or loads, compared to the quasi-static hardness. For copper, while the quasi-static SEM hardness without CSM oscillation shows a strong "smaller being stronger" indentation size effect, the hardness with CSM

amplitudes ≥ 4nm exhibits no increasing trend as the indent size decreases, and that with CSM amplitude of 2nm exhibits a weaker indent size effect. For molybdenum, although all the data exhibit indentation size effect, this effect diminishes at increasing CSM vibration amplitudes.

It is also interesting to see the extent of hardness reduction in vibrated indentation relative to the hardness without vibration. Therefore, in Fig. 6, the hardness reduction values (H-H_o), which are the SEM hardness obtained in vibrated experiments minus that obtained in quasi-static experiments at the same depth, are calculated and plotted against the target indent depth to amplitude ratio in log scale. Since the same amplitude should have a greater effect at smaller indent depths, and also the magnitudes of vibration used for macroscopic indentation are very different from those used in nanoindentation, the target depth is normalized by the vibration amplitude for better comparison. For the macroscopic indents, their diagonal lengths are divided by 7 to obtain the vertical depth of each indent, and this is then normalized by the vibration amplitude of 2 μm used in the tests. Fig. 6(a) and (b) show the results for copper and molybdenum respectively, and for comparison purposes, the results for aluminium calculated using data from our previous studies [41, 42] are also presented in Fig. 6(c). In all cases, it can be seen that the hardness reduction is minimal for

log(target-indent-depth/amplitude) larger than about 2, but below this value, the magnitude of hardness reduction, (H_o-H), increases almost linearly with decreasing log(target indent depth/amplitude). It can also be seen that although the amplitudes and frequencies used in the macro- and nanoindentation tests are very different, their hardness reduction values roughly fall in the same trend; the small discrepancies may be due to the fact that in the macro-indentation case the ultrasound vibration is applied horizontally, while in the nanoindentation case the CSM vibrations are axial. The hardness reduction phenomenon induced by vibrations is therefore common for all the three metals studied.

Fig. 7(a) and (b) are cross-sectional TEM montages of nanoindents made with the quasi-static mode and CSM mode with 12 nm amplitude at 45 Hz respectively for copper, and Fig. 7(c) and (d) show their counterparts for molybdenum. As is different from the aluminium nanoindents observed in [42], no obvious subgrains can be observed in these samples. Although subgrain formation is not obvious in the vibrated nano-indents in Cu and Mo, a significant difference in dislocation density can still be observed when compared to the non-vibrated case. The insets in Fig. 7(a) to (d) show magnified regions of the corresponding montages, and since the samples were tilted close to the Bragg condition in order to show the dislocations in the selected locations,

the inset may look different from the unmagnified picture. Fig. 7(a) shows that for copper the dislocation density in the non-vibrated indent is about 10^{15} m^{-2} while Fig. 7(b) shows the dislocation density of the vibrated indent is about 10^{14} m^{-2}. Also, for molybdenum, the dislocation density in the vibrated indent is 10^{13} m^{-2}, while that in the non-vibrated one is lower at 10^{14} m^{-2}. In both materials, the dislocation density in the vibrated indents was about one order of magnitude lower than the non-vibrated state.

4. Discussion

From Fig. 1 it can be seen that for copper and molybdenum a small vibration with 2 μm amplitude can cause a large increase in the indent's diagonal length by more than 80 μm. Fig. 2 and 3 also show clearly that significant subgrain formation occurs with decrease in dislocation density in these samples, and indentation alone without vibration did not trigger subgrain formation. These effects are similar to those observed in aluminium [41], indicating that the observed phenomena of ultrasound excitation intrinsically changing the resistance to deformation through enhancing subgrain formation occur in different metals with different SFE and crystal structures.

Nanoindentation results of copper and molybdenum also show similarities to those of aluminium [42], in that lowering of loading can be observed in the

load-displacement curves (Fig. 4) and hardness is reduced at low indent depths compared with quasi-static nanoindentation (Fig. 5). SEM hardness in eqn. (1) instead of the hardness value given by the CSM protocol is used here as a direct measure of the mean pressure underneath the indenter, and for self-similar indenter shapes this should be independent of the indentation force, if the material does not exhibit intrinsic mechanisms that would destroy the self-similarity condition. Thus, the observed softening is not caused by load superposition, and the material's intrinsic resistance to deformation does change with a simultaneous oscillatory force. The intrinsic change also tallies well with the observed microstructural changes from the TEM pictures shown in Fig. 7, in that the dislocation density for vibrated indents is significantly smaller than the non-vibrated states.

Fig. 6(a) to (c) show a comparison on macroscopic and nanometric deformation with vibration, the reductions of hardness in different scales roughly fall into the same trend, despite the huge differences in vibration frequencies and amplitudes. This shows that the softening effect due to vibration is of a similar nature and should be due to similar microscopic mechanisms.

The similarities mentioned above show that the vibration induced softening observed in this study is of the same nature as those in previous studies [41, 42], and can be explained by the periodic reversal or slowing down of motions of dislocations caused by the oscillatory stress, to allow dislocations to explore more and hence increase their chance of dipole annihilation [43]. The dislocation annihilation rate $\dot{\rho}_{ann}$ can be expressed as

$$\dot{\rho}_{ann} = \rho \nu_a \exp\left[-Q(\sigma)/kT\right] \tag{3}$$

where ρ is the mobile dislocation density, $\exp\left[-Q(\sigma)/kT\right]$ the usual Boltzmann factor for annihilation which depends on stress σ and temperature, and ν_a an "attempt" frequency which denotes the frequency for a given dislocation to meet a suitable partner for annihilation. With an oscillatory stress superimposing, the motions of dislocations are periodically slowed down or even reversed during the half cycles when the oscillatory stress opposes the quasi-static applied stress, and the conjecture here is that in a mutually interactive environment, such jerky or reversal nature of dislocation motion can cause the attempt frequency ν_a above to increase significantly. Such a mechanism is supported by dislocation dynamics simulations [43], and the present observations on reduced dislocation density in Cu and Mo (Figs. 3 and 7), together with similar observations on Al [41,42], suggest that vibration-induced enhancement of dislocation annihilation is a rather universal phenomenon that can

happen in metals with different SFE and crystal structures. With promoted annihilation, the flow stress should decrease due to reduced strain-hardening, and this is thought to be the major reason for the observed softening caused by vibrations.

Although the enhancement of dislocation annihilation is a rather general feature induced by vibrations, enhancement of subgrain formation is more complicated. Figs. 2 and 3 indicate clearly the enhancement of subgrain formation in vibrated macro-indents in Cu and Mo, and similar observations were made in Al beforehand [41]. However, in the case of CSM nanoindentation, earlier observations indicate subgrain enhancement in Al [42], but Fig. 7(b) and (d) here show no obvious subgrain formation in Cu and Mo. This shows that when the strain gradients are smaller as in the case of macro-indents, the vibration-induced enhancement of dislocation annihilation is accompanied by subgrain formation in all three metals studied, but subgrain formation in the high strain-gradient situations in nanoindentation is dependent on the material's crystal structure as well as SFE. The high SFE of aluminium allows its dislocations to cross-slip more frequently resulting in easy dislocation annihilation and subgrain formation even in high strain-gradient situations, but for copper with lower SFE [45], cross-slip is less easy and so only dislocation annihilation, but no obvious subgrain formation, occurs in nanoindentation. The TEM observations here match the DD

simulation results that dislocation annihilation is affected by the ease of cross-slip [43]. The absence of subgrain in molybdenum during CSM nanoindentation suggests that the subgrain formation is also more difficult in a BCC metal.

For both copper and molybdenum, the hardness obtained with CSM nanoindentation is reduced relative to the quasi-static hardness obtained at the same depth, as shown in Fig. 6, and the amount of reduction depends on depth and vibration amplitude. However indentation size effect can still be observed in some of the tests for copper, and in all the tests for molybdenum. Fig. 5 also shows that the “smaller being stronger” size effect competes with the “smaller being softer” softening effect of the vibration, and the result of this wrestle determines whether an overall softening or hardening can be observed at low depths. Comparing to aluminium [42] in all cases, copper and molybdenum are less easy to be softened at the same vibration condition, and the TEM observation in Fig. 7 is actually reflecting the less extent of softening induced by the vibration in copper and molybdenum under the same condition. The extent of softening and subgrain formation should be dependent on dislocation mobility, cross-slip ability and crystal structure that can affect dislocation annihilation and thus the resultant softening effect. Furthermore, the effect of nanometric oscillations on

different metals during nanomechanical deformation is still an open topic at the moment, and more work deserves to be done in the future.

5. Conclusions

Macroscopic and nanoindentation were performed on copper and molybdenum. In both macro- and nano-length scales, indentation was performed in both quasi-static mode alone and with oscillatory loadings superimposed on the samples. It was found that simultaneous application of oscillations can intrinsically lower the hardness of these samples. EBSD and TEM observations show that reduction in dislocation density and/or subgrain formation generally occur with simultaneous application of oscillations in both metals studied. Together with similar phenomena previously observed from aluminium, it is concluded that the softening effect induced by vibrations is a general, intrinsic phenomenon that tallies well with enhanced dislocation annihilation and/or subgrain formation.

Acknowledgment

The work described in this paper was supported by grants from the Research Grants Council (Project No. 7159/10E) as well as from the University Grants

Committee (Project No. SEG-HKU06) of the Hong Kong Special Administrative Region.

References

[1] B. Langenecker, AIAA J. 1 (1963) 80-83.

[2] B. Langenecker, IEEE Trans. Son. Ultrason. 1 (1966) 1-8.

[3] K.C. Joshi, Weld J. 50 (1971) 840-848

[4] K.F. Graff, IEEE Trans. Son. and Ultrason. SU22 (1975) 234-234.

[5] A.E. Eaves, A.W. Smith, W.J. Waterhouse, D.H. Sansome, Ultrasonics 13 (1975) 162-170.

[6] H. Kreye, M. Hammerschmidt, G. Reiners, Scripta Metall. 12 (1978) 1059-1061.

[7] R. Neugebauer and A. Stoll, J. Mater. Process Technol. 149 (2004) 633-639.

[8] C. Zhang, R. Rentsch, E. Brinksmeier, Int. J. Mach. Tool. Manu. 45 (2005) 881-890.

[9] B.N. Mordyuk and G.I. Prokopenko, J. Sound Vibrat. 308 (2007) 855-866.

[10] D.E. Brehl and T.A. Dow, Precis. Eng. 32 (2008) 153-172.

[11] W. Mason, Bell Syst. Tech. J. 34 (1955) 903-907.

[12] G. E. Nevill and F. Brotzen, Proc. Am. Soc. Testing Materials 57 (1957) 751-755.

[13] O. Izumi, K. Oyama, Y. Suzuki, Trans. Jpn. Inst. Metals 7 (1966) 158-162.

[14] O. Izumi, K. Oyama, Y. Suzuki, Trans. Jpn. Inst. Metals 7 (1966) 162-166.

[15] G. S. Baker and S. H. Carpenter, J. Appl. Phys. 38 (1967) 1586-1591.

[16] T .Endo, K. Suzuki, M. Ishikawa, Trans. Jpn. Inst. Metals 20 (1979) 706-712.

[17] H. O. K. Kirchner, W. K. Kromp, F. B. Prinz, P. Trimmel, Mater. Sci. Eng. 68 (1985) 197-206.

[18] T. Ohgaku and N. Takeuchi, Phys. Status Solidi. A 111 (1989) 165-172.

[19] K. V. Sapozhnikov and S. B. Kustov, Phil. Mag. A 76 (1997) 1153-1168.

[20] K.V. Sapozhnikov, S.N. Golyandin, S.B. Kustov, Phil. Mag. A 77 (1998) 151-166.

[21] K.V. Sapozhnikov, S.N. Golyandin, S.B. Kustov, J. Van Humbeeck, R. De Batist, Acta Mater. 48 (2000) 1141-1151.

[22] Z. Huang, M. Lucas, M. J. Adams, Ultrasonics 40 (2002) 43-48.

[23] Z. Huang, M. Lucas, M. J. Adams, Proc. SPIE Int. Soc. Opt. Eng. 4537 (2002) 445-448.

[24] J.-C. Hung and C. Hung, Ultrasonics 43 (2005) 692-698.

[25] J-C. Hung, Y-C. Tsai, C. Hung, Ultrasonics 46 (2007) 277-284.

[26] Y. Daud, M. Lucas, Z. Huang, Ultrasonics 44 (2006) e511–e515.

[27] Y. Daud, M. Lucas, Z. Huang, J. Mater. Process Technol. 186 (2007) 179-190.

[28] J.E. Krzanowski, IEEE Trans. Compon. Hybrids Manuf. Technol. 13 (1990) 176-181.

[29] J.B. Pethica and W.C. Oliver, Mater. Res. Soc. Symp. Proc. 130 (1989) 13-23.

[30] W.C. Oliver and G.M. Pharr, J. Mater. Res. 7 (1992) 1564-1583.

[31] S.A.S. Asif K.J. Wahl and R.J. Colton, Rev. Sci. Instrum. 70 (1999) 2408-2413.

[32] X. Li and B. Bhushan, Mater. Char. 48 (2002) 11-36.

[33] W.C. Oliver and G.M. Pharr, J. Mater. Res. 19 (2004) 3-20.

[34] K. Durst, O. Franke, A. Bohner and M. Goken, Acta Mater. 55 (2007) 6825-6833.

[35] M.J. Cordill, N.R. Moody and W.W. Gerberich, J. Mater. Res. 23 (2008) 1604-1613.

[36] M.J. Cordill, N.R. Moody and W.W. Gerberich, Int. J. Plast. 25 (2009) 281-301.

[37] M.J. Cordill, M.S. Lund, J. Parker, C. Leighton, A.K. Nair, D. Farkas, N.R. Moody and W.W. Gerberich, Int. J. Plast. 25 (2009) p.2045.-2058.

[38] G.M. Pharr, J.H. Strader and W.C. Oliver, J. Mater. Res. 24 (2009) 653-666.

[39] M. Tanibayashi, Phys. Status Solidi 128 (1991) 83-94.

[40] G.A. Malygin, Phys. Solid State 42 (2000) 69-75.

[41] K.W. Siu, A.H.W. Ngan and I.P. Jones, Int. J. Plast 27 (2011) 788-800.

[42] K.W. Siu and A.H.W. Ngan, Phil. Mag. 93 (2013) 449-467.

[43] K.W. Siu and A.H.W. Ngan, Phil. Mag. 91 (2011) 4367-4387.

[44] A.C. Fischer-Cripps, Nanoindentation, second ed., Springer, New York, 2004.

[45] R.E. Smallman and A.H.W. Ngan, Physical Metallurgy and Advanced Materials, seventh ed., Butterworth-Heinemann, Oxford, 2007.

Figure Captions

Fig. 1 Indent diagonal length and Vickers hardness vs sample's vibration amplitude for different indenter tip loadings for (a) copper and (b) molybdenum. The error bars account for one standard deviation of data scattering.

Fig. 2 EBSD orientation map of cross-sectional foils cut from indents made by 0.05 kg load of (a) copper without vibration, (b) copper with 2 μm vibration, (c) molybdenum without vibration, (d) molybdenum with 2 μm vibration.

Fig. 3 TEM montages of parts of cross-sectional foils cut from indents made by 0.05 kg load of (a) copper without vibration, (b) copper with 2 μm vibration, (c) molybdenum without vibration, (d) molybdenum with 2 μm vibration.

Fig. 4 Representative load-displacement curves under quasi-static mode and CSM mode at 45 Hz with different amplitudes for (a) copper (b) molybdenum.

Fig. 5 SEM hardness versus the target indent depth of quasi-static and CSM nanoindentation with amplitudes of 2nm, 4 nm, 8 nm and 12 nm for (a) copper and (b)

molybdenum.. Data in the “wookpecker” regime of depth/amplitude are circled. The error bars account for one standard deviation of data scattering.

Fig. 6 Hardness reduction values H-H_o versus target indent depth to amplitude ratio in log scale for (a) copper, (b) molybdenum and (c) aluminium. The results for aluminium are calculated using data in previous studies [41, 42].

Fig. 7 Cross-sectional TEM montages of nanoindents made with (a) quasi-static mode on copper, (b) CSM mode of amplitude 12 nm at 45 Hz on copper, (c) quasi-static mode on molybdenum, (d) CSM mode of amplitude 12 nm at 45 Hz on molybdenum.

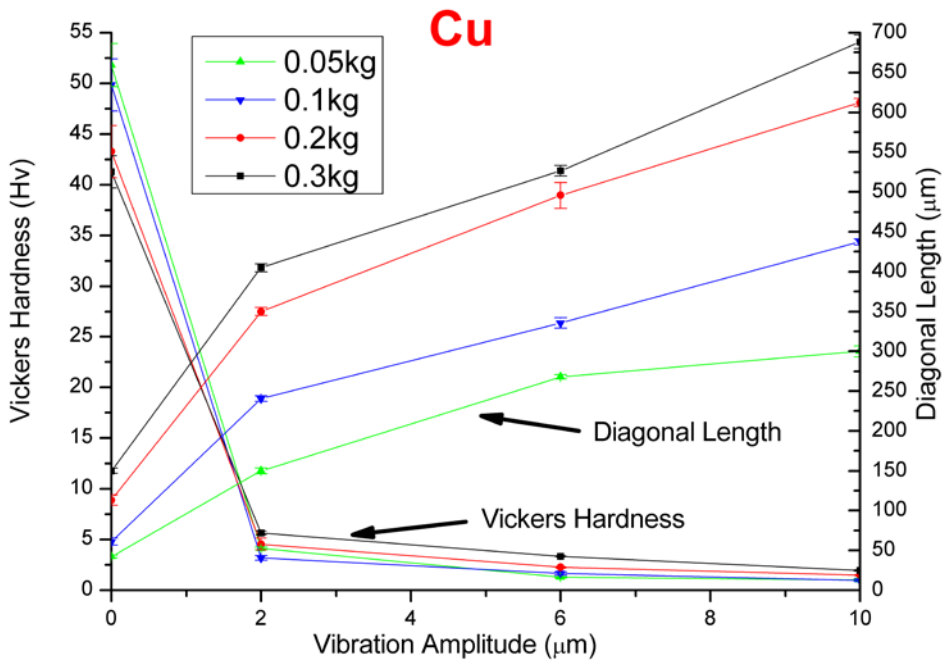
Cu
0.05kg
0.1kg
0.2kg
0.3kg
Vickers Hardness (Hv)
Diagonal Length (μm)
Vibration Amplitude (μm)
Diagonal Length
Vickers Hardness

(a)

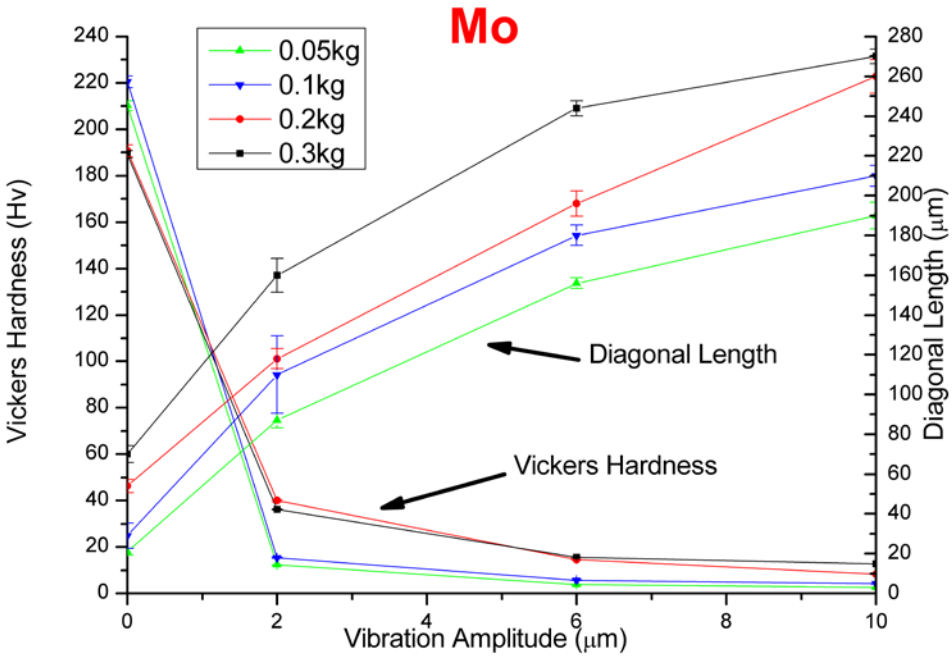
Mo
0.05kg
0.1kg
0.2kg
0.3kg
Vickers Hardness (Hv)
Diagonal Length (μm)
Vibration Amplitude (μm)
Diagonal Length
Vickers Hardness

(b)

Fig. 1

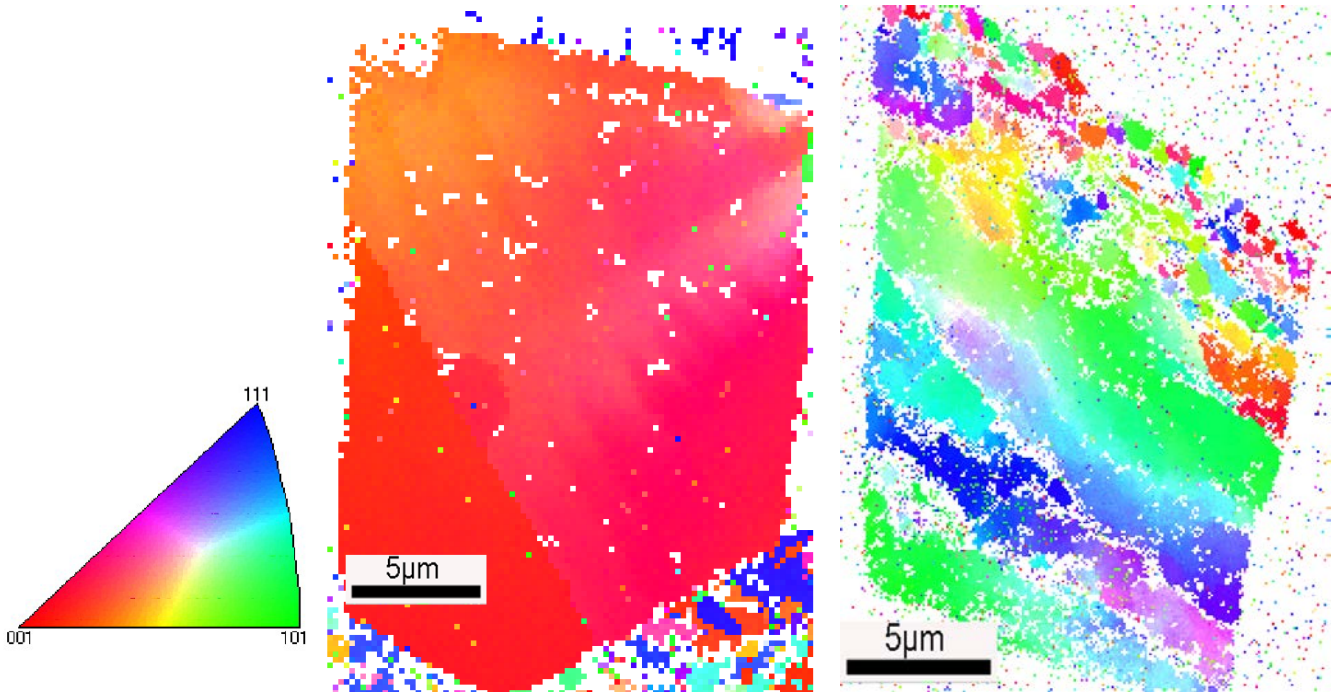

(a) (b)

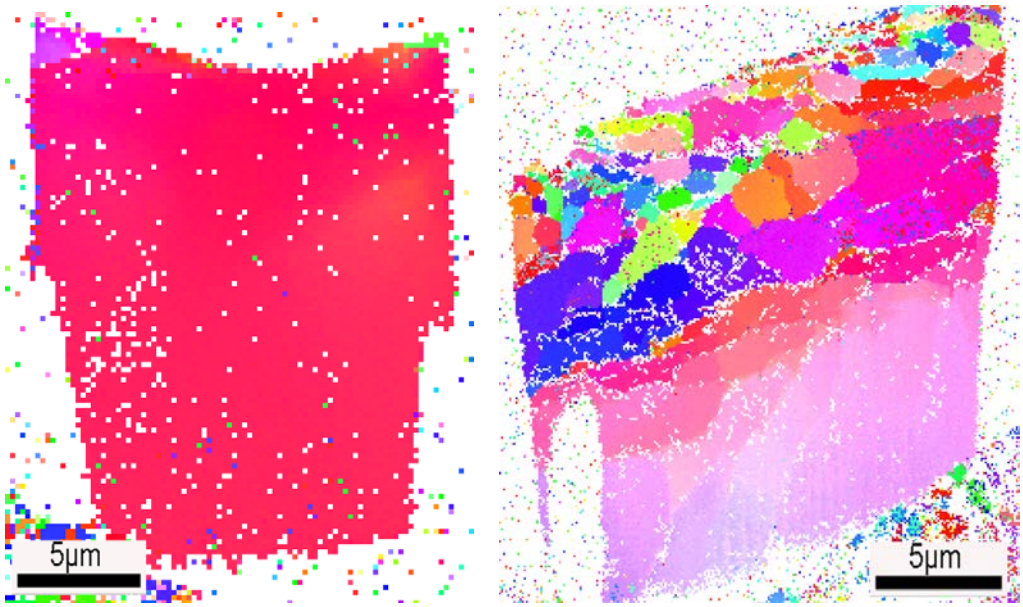

(c) (d)

Fig. 2

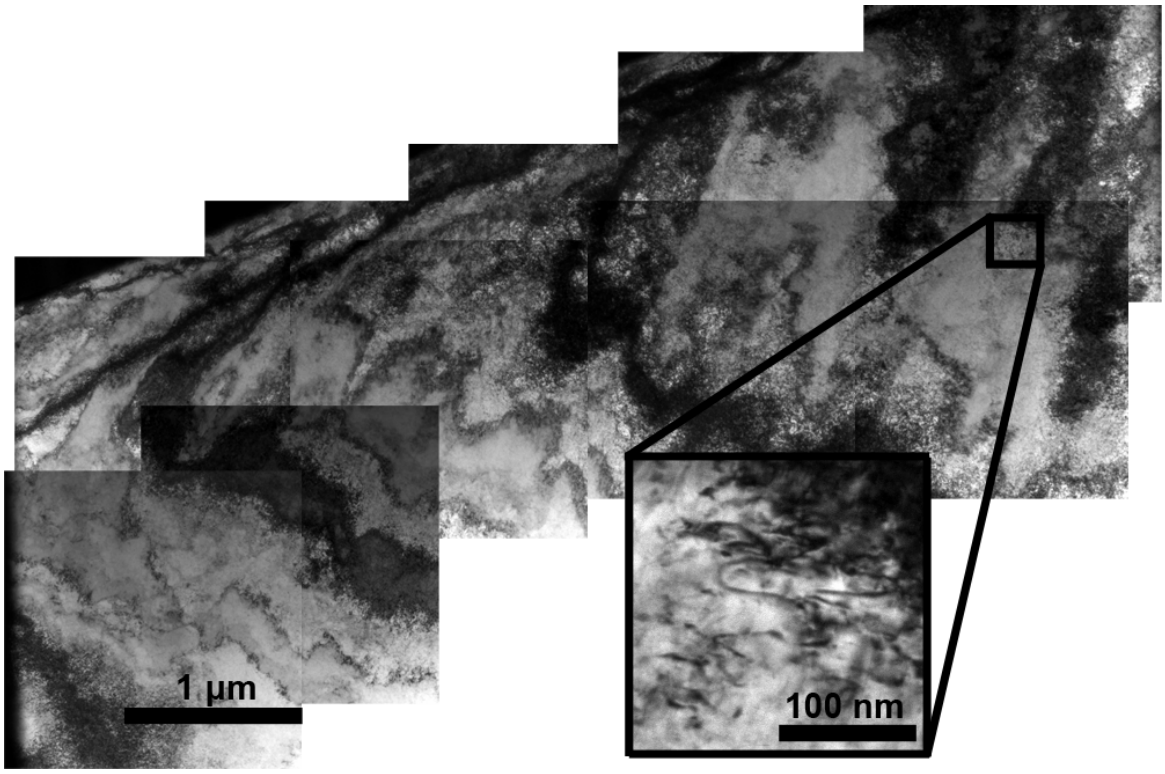

(a)

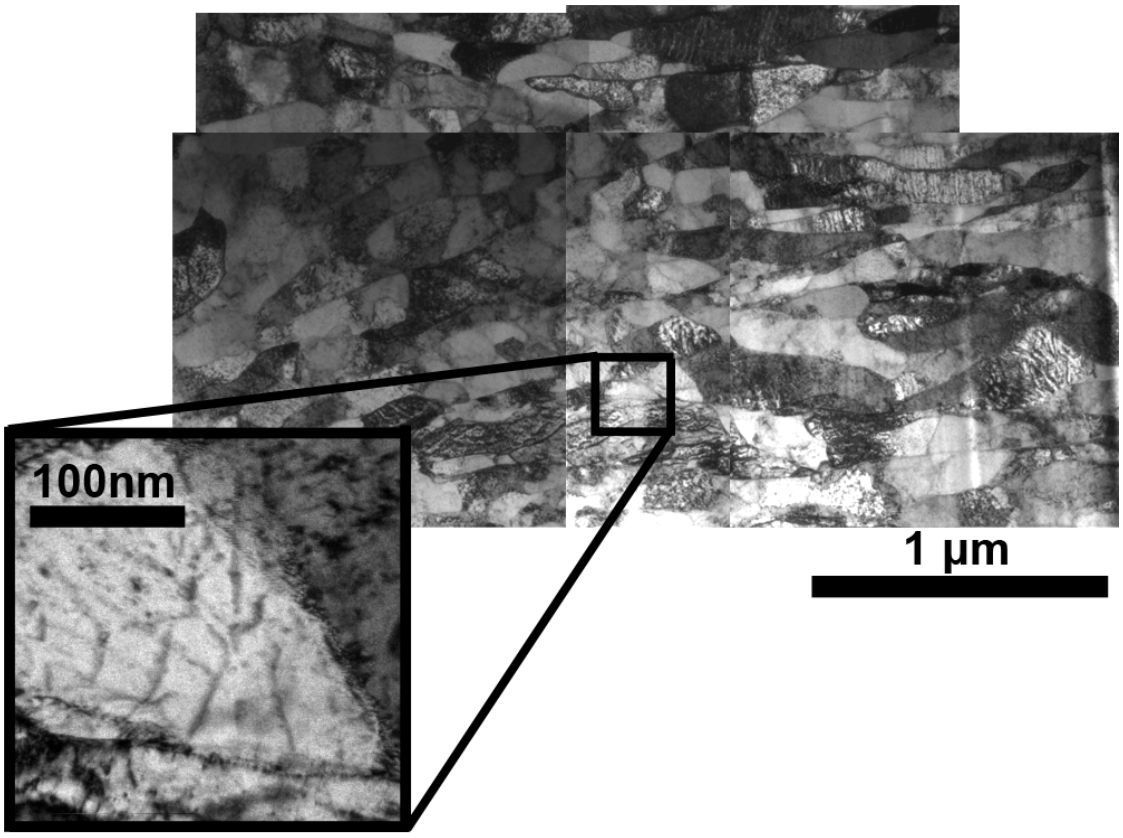

(b)

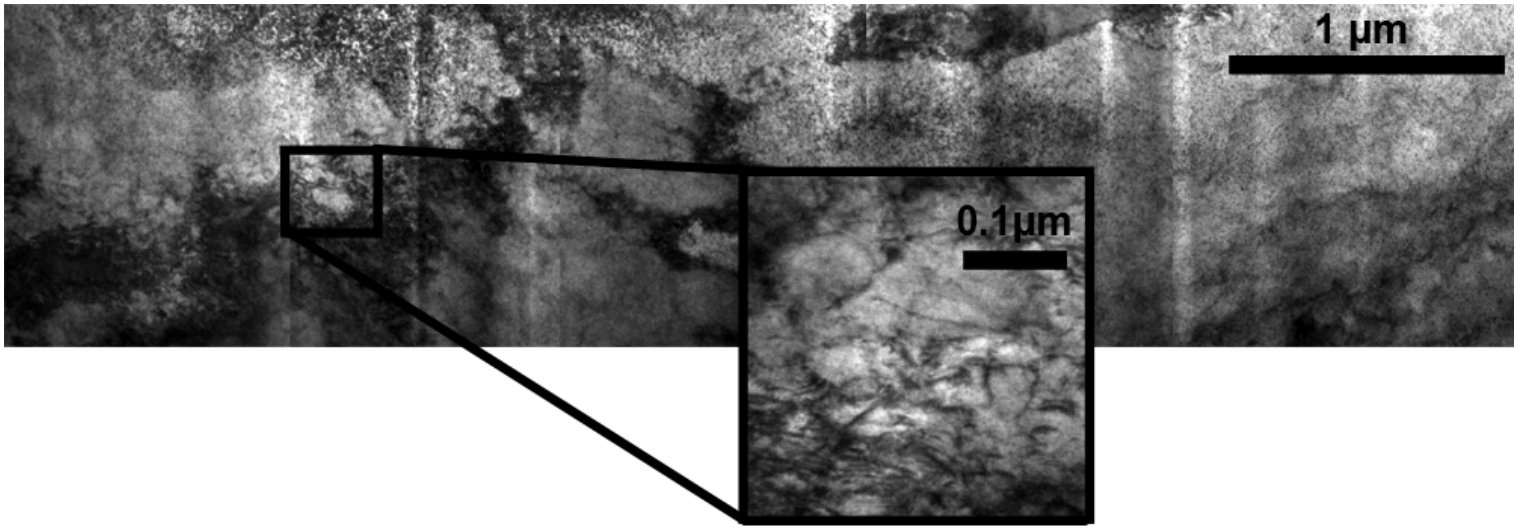

(c)

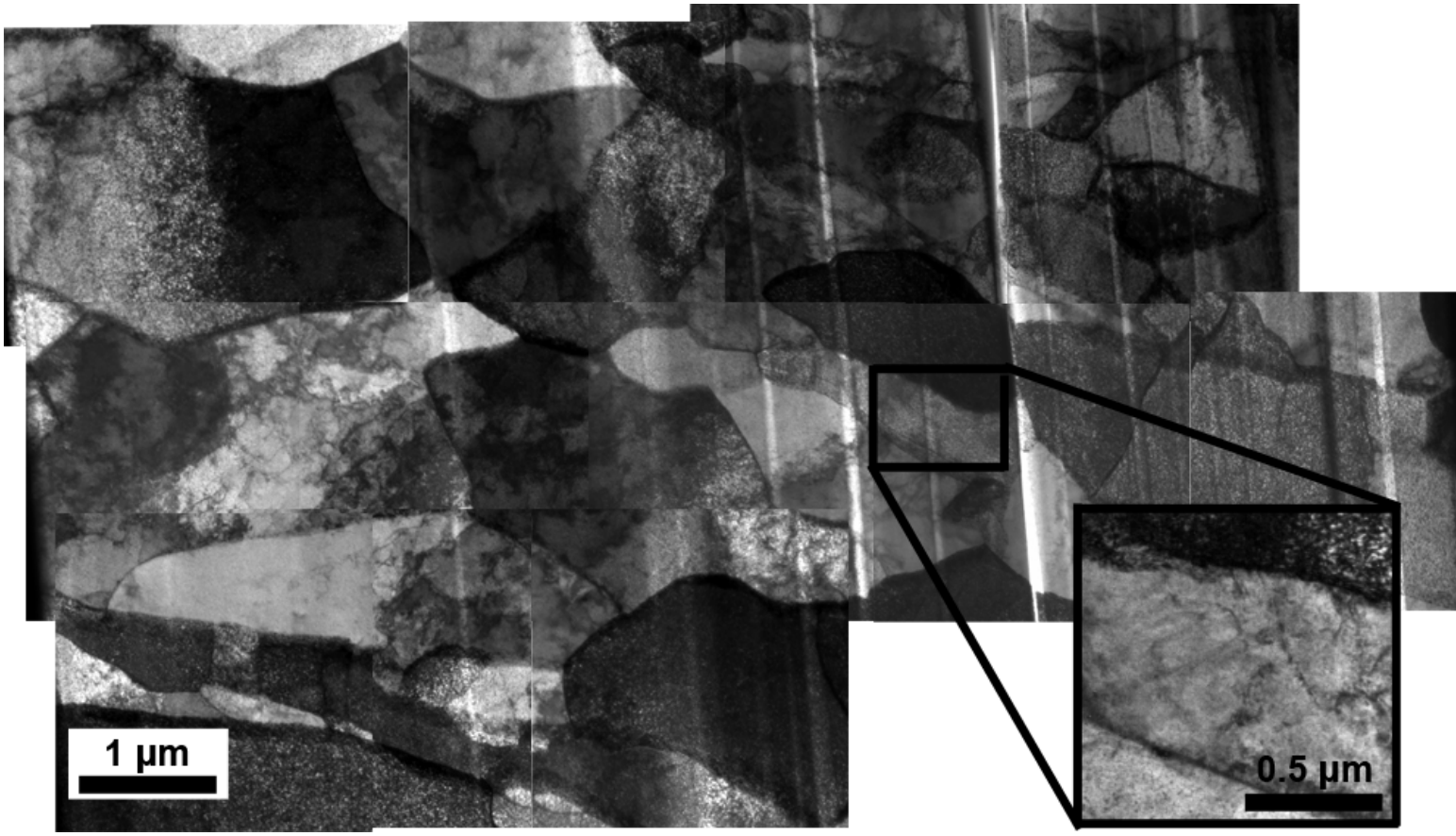

(d)

Fig. 3

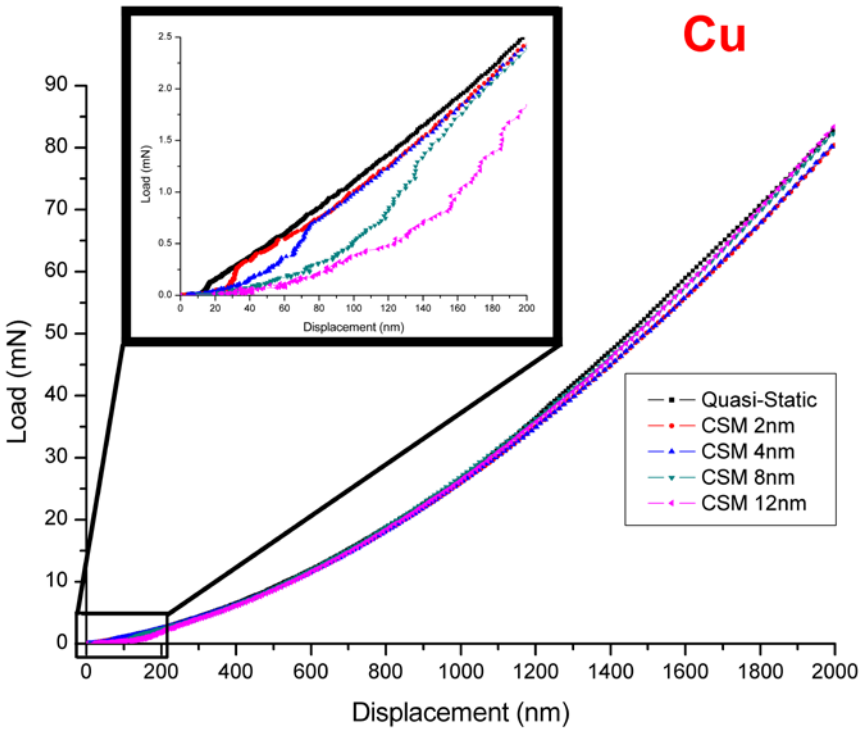
Cu
Load (mN)
Displacement (nm)
Quasi-Static
CSM 2nm
CSM 4nm
CSM 8nm
CSM 12nm

(a)

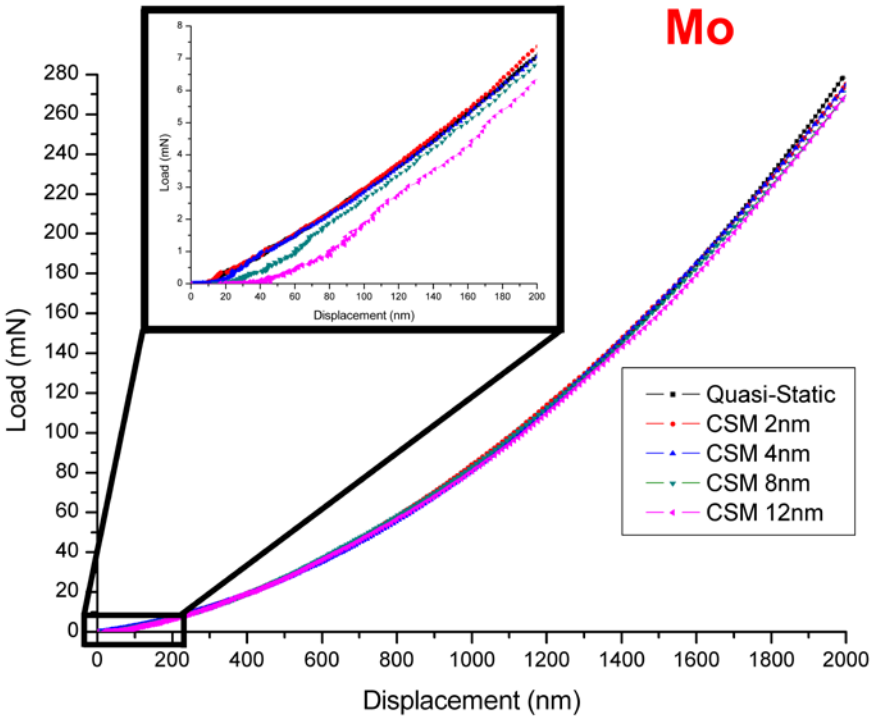
Mo
Load (mN)
Displacement (nm)
Quasi-Static
CSM 2nm
CSM 4nm
CSM 8nm
CSM 12nm

(b)

Fig. 4

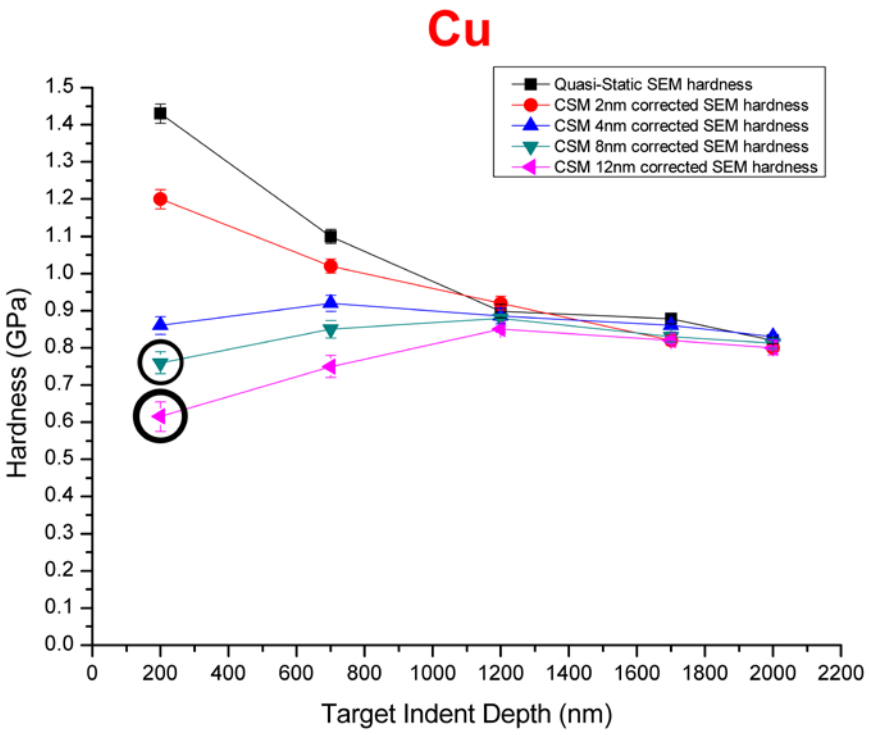
Cu
Quasi-Static SEM hardness
CSM 2nm corrected SEM hardness
CSM 4nm corrected SEM hardness
CSM 8nm corrected SEM hardness
CSM 12nm corrected SEM hardness
Hardness (GPa)
Target Indent Depth (nm)

(a)

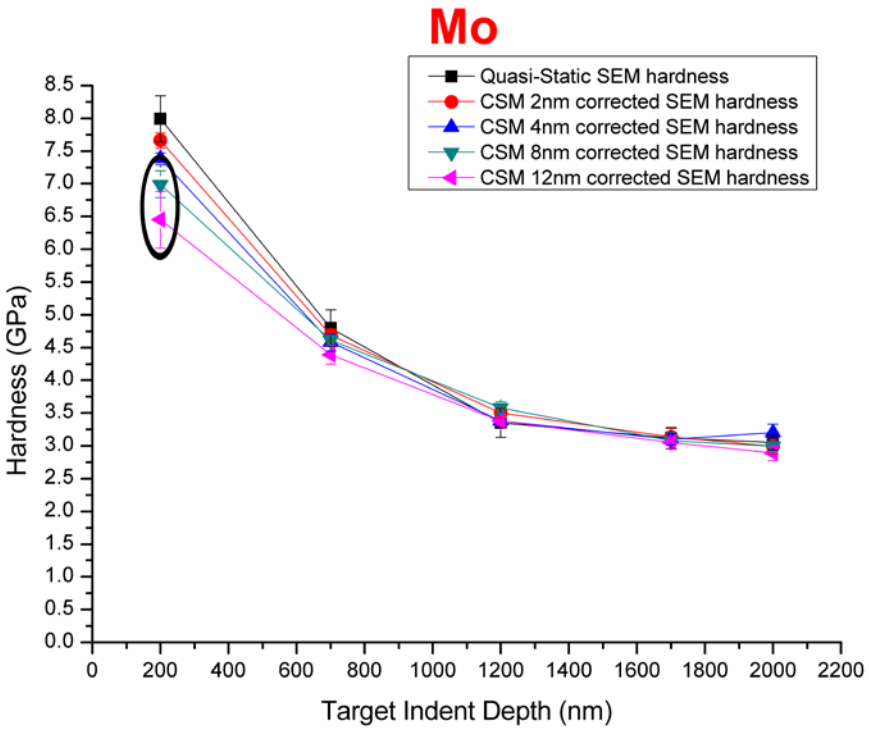
Mo
Quasi-Static SEM hardness
CSM 2nm corrected SEM hardness
CSM 4nm corrected SEM hardness
CSM 8nm corrected SEM hardness
CSM 12nm corrected SEM hardness
Hardness (GPa)
Target Indent Depth (nm)

(b)

Fig. 5

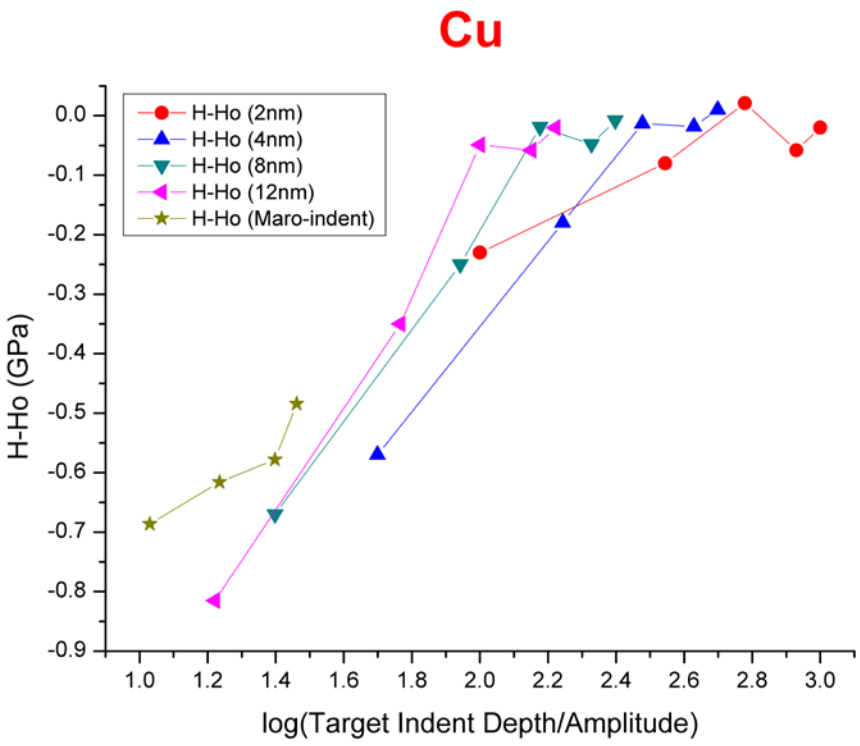
Cu
H-Ho (2nm)
H-Ho (4nm)
H-Ho (8nm)
H-Ho (12nm)
H-Ho (Maro-indent)
H-Ho (GPa)
0.0
-0.1
-0.2
-0.3
-0.4
-0.5
-0.6
-0.7
-0.8
-0.9
1.0
1.2
1.4
1.6
1.8
2.0
2.2
2.4
2.6
2.8
3.0
log(Target Indent Depth/Amplitude)

(a)

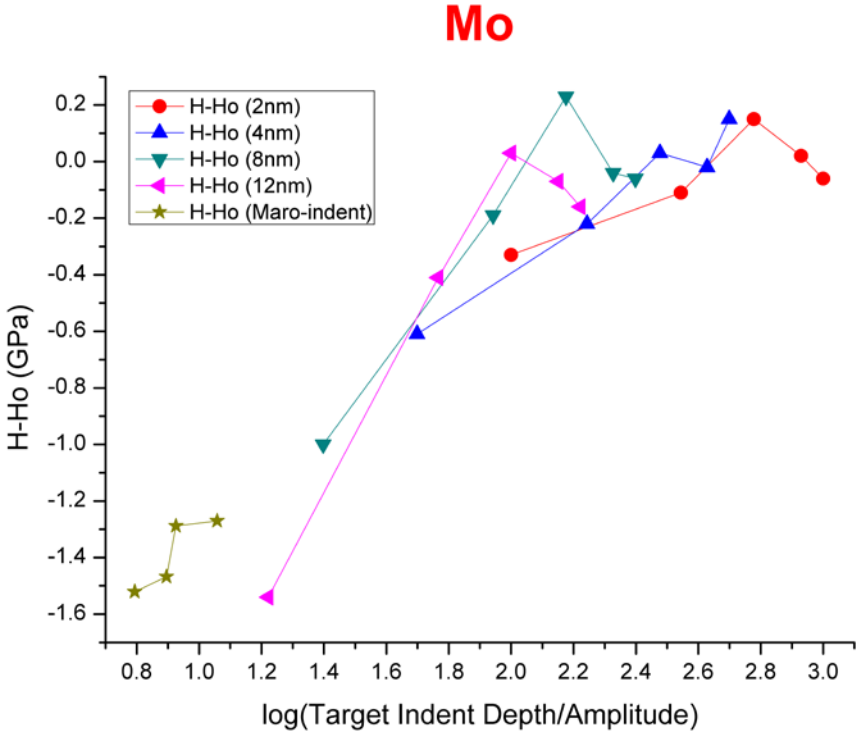
Mo
H-Ho (2nm)
H-Ho (4nm)
H-Ho (8nm)
H-Ho (12nm)
H-Ho (Maro-indent)
H-Ho (GPa)
0.2
0.0
-0.2
-0.4
-0.6
-0.8
-1.0
-1.2
-1.4
-1.6
0.8
1.0
1.2
1.4
1.6
1.8
2.0
2.2
2.4
2.6
2.8
3.0
log(Target Indent Depth/Amplitude)

(b)

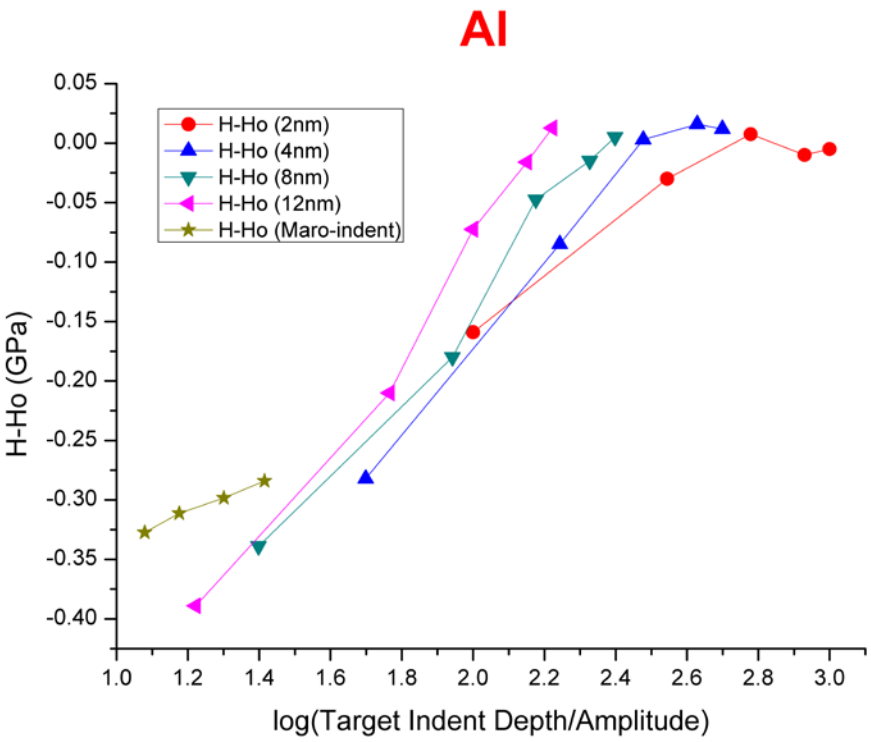
Al
H-Ho (2nm)
H-Ho (4nm)
H-Ho (8nm)
H-Ho (12nm)
H-Ho (Maro-indent)
H-Ho (GPa)
0.05
0.00
-0.05
-0.10
-0.15
-0.20
-0.25
-0.30
-0.35
-0.40
1.0
1.2
1.4
1.6
1.8
2.0
2.2
2.4
2.6
2.8
3.0
log(Target Indent Depth/Amplitude)

(c)

Fig. 6

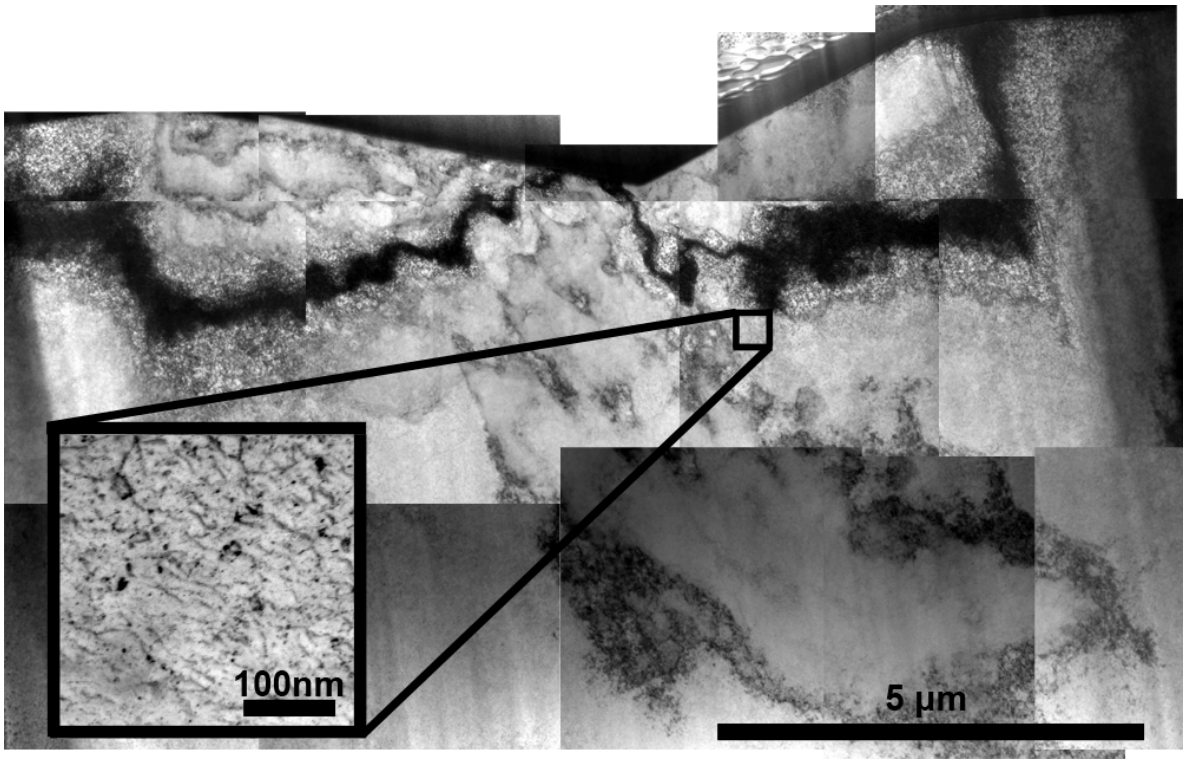

(a)

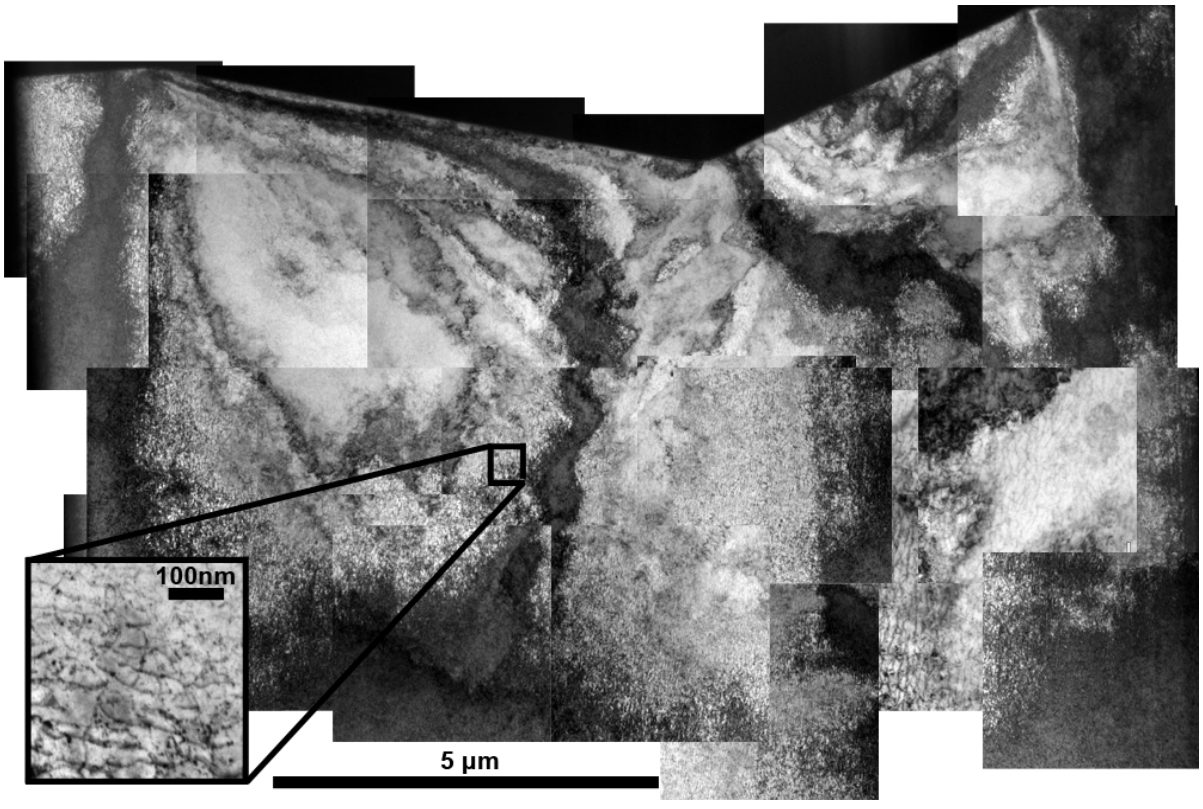

(b)

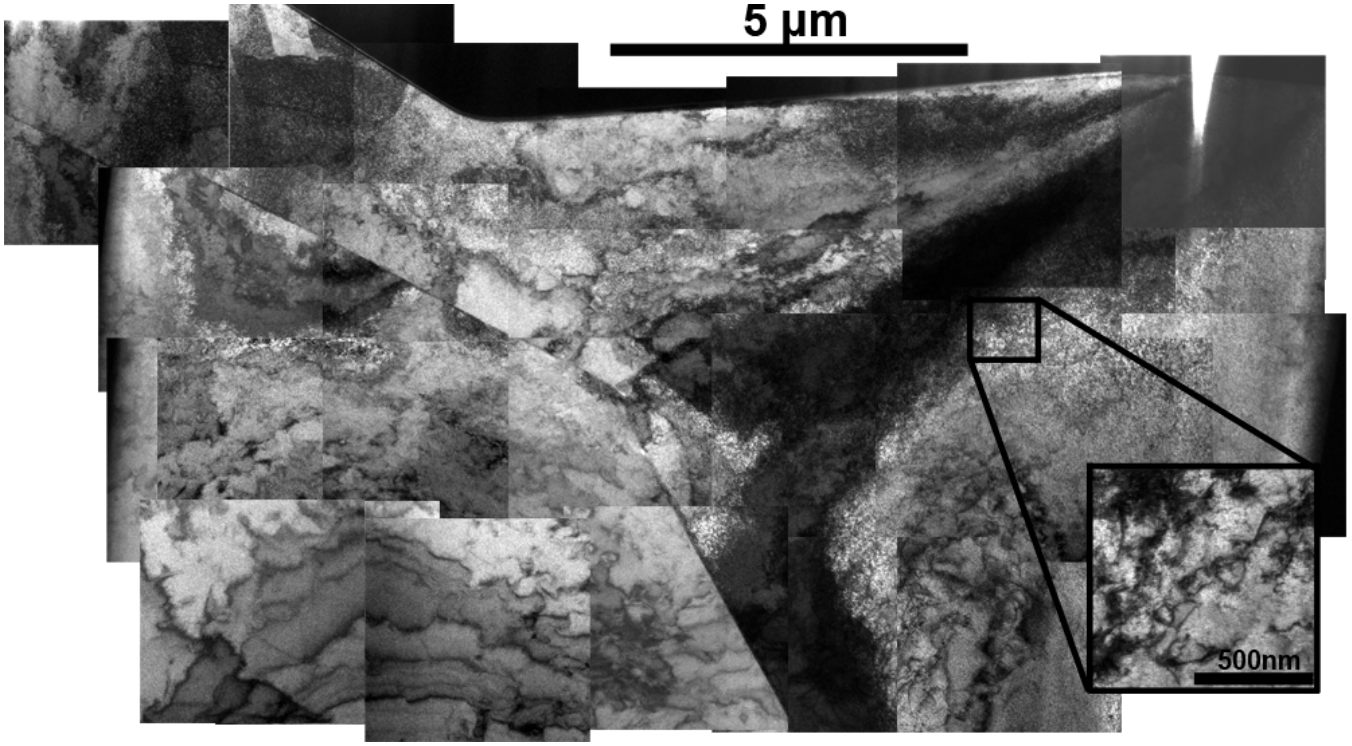

(c)

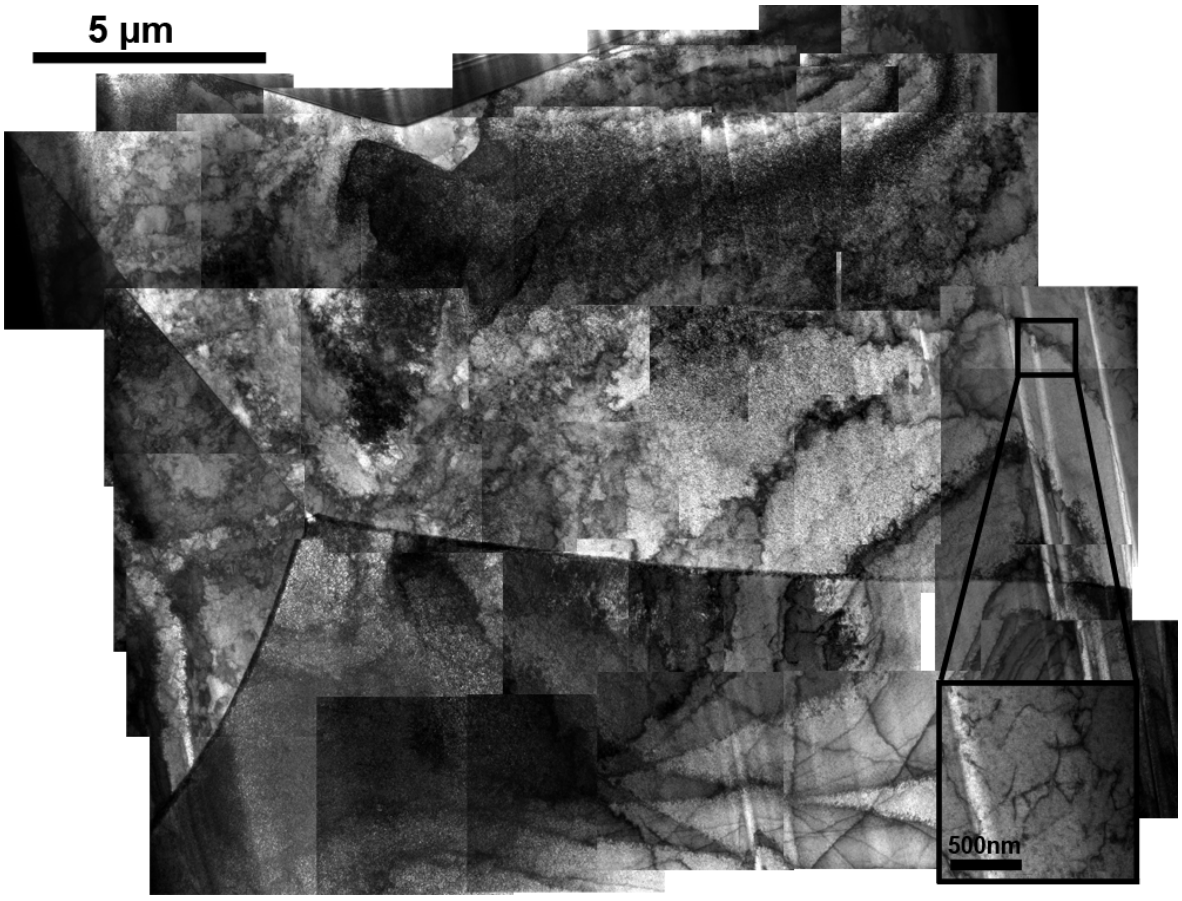

(d)

Fig. 7